

Wavevector multiplexed quantum memory as a universal platform for quantum state preparation

M. Parniak^{1,†}, M. Dąbrowski^{1,*}, M. Mazelanik¹, A. Leszczyński¹, M. Lipka¹, and W. Wasilewski¹

¹*Institute of Experimental Physics, Faculty of Physics,
University of Warsaw, Pasteura 5, 02-093 Warsaw, Poland*

Parallelized quantum information processing requires tailored quantum memories to simultaneously handle multiple photons. The spatial degree of freedom is a promising candidate to facilitate such photonic multiplexing. Using a single-photon resolving camera we demonstrate a wavevector multiplexed quantum memory based on a cold atomic ensemble. Observation of nonclassical correlations between Raman scattered photons is confirmed by a value of the second-order correlation function $g_{S,AS}^{(2)} > 80$ in an unprecedented number of 665 separated modes simultaneously. Our scheme is perfectly matched to expedite quantum communication in free-space or with multimode fibers, as well as quantum imaging and image processing at the single-photon level. Moreover, we propose a protocol utilizing the multimode memory along with the camera to facilitate generation of multi-photon states, which are a necessity in quantum-enhanced sensing technologies and as an input to photonic quantum circuits.

Multiplexing in optical fibers or in free-space is essential in modern techniques for high-throughput transmission^{1,2}. Similarly, as quantum technologies mature, the necessity of multiplexing in photon-based quantum communication becomes clear³ and much effort is devoted to various schemes exploiting spatial^{4–11} or temporal^{12–17} degrees of freedom. Utilization of many modes can finally allow efficient application of the Duan-Lukin-Cirac-Zoller (DLCZ) protocol^{18–21} and offer nearly-deterministic generation of multi-photon states^{22–24} later applicable in quantum enhanced sensing technologies^{25,26} as well as optical quantum computation²⁷.

Regardless of substantial efforts, the task of achieving large number of modes remains a challenging endeavor especially in hybrid atom-photon systems. In purely photonic, memoryless systems hundreds of modes have been obtained within the spatial domain of spontaneous parametric down-conversion (SPDC)^{28–30} or by means of frequency-time entanglement^{17,31–35}. However, most applications such as the DLCZ protocol¹⁸, enhanced photon generation^{23,24,36} or even linear optical quantum computing (LOQC)²⁷ require or greatly benefit from a multimode quantum memory. For instance, the largest number of temporal modes used for photon storage in cavity-based quantum memory³² is 30. Likewise, ensembles of dopants in crystals have been used to store externally generated photons³⁷ in up to 100 modes or otherwise generate them^{20,21} in 12 modes. Another mainstream trend is to build a multiplexed quantum repeater by splitting a trapped atomic ensemble into many cells^{5,23}. The idea was recently realized in two dimensions achieving 225 modes³⁸. These schemes however suffer from the limitation given by difficulty in trapping large ensembles as well as hinder heralded simultaneous excitation of all modes. In consequence, they are rendered useful only for the DLCZ quantum repeater¹⁸ but neither for quantum imaging^{39–41} nor enhancing rate of the photonic state generation^{23,24}.

The purpose of this paper is a demonstration of massive improvement in the number of modes processed by the quantum memory. The experimental realization is accomplished through multiplexing of angular emission modes of a single quantum memory and by employing a spatially-resolved single-photon detection. Our experiment greatly exceeds the capacity of previous approaches by generating photons in 665 pairwise-coupled modes, exploring the previously intangible regime of multimode capacity with simultaneous extremely low noise-

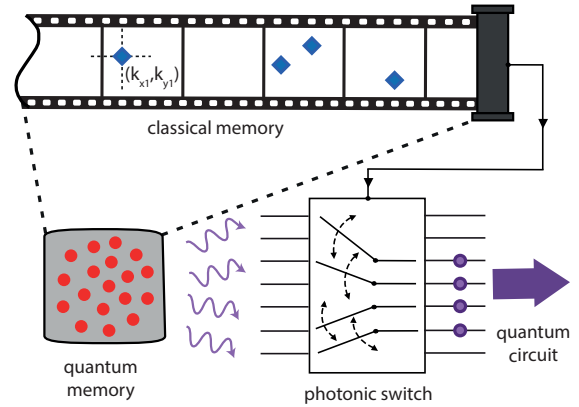


Figure 1. Single photon spatial routing and multiplexing for multi-photon state generation. A single-photon resolving camera registers consecutive frames during the quantum memory write-in process. Each detection heralds creation of a spin-wave excitation in the atomic ensemble quantum memory with a wavevector determined by the position (k_{xi}, k_{yi}) at which i -th photon was registered. Acquisition and write-in continues until the desired number of excitations has been created. At this time a photonic switch is reconfigured to channel photons from conjugate directions stored in a classical memory and subsequently the readout pulse is applied to convert stored spin-wave excitations to the requested number of photons, which will be used later, e.g. in the quantum circuit.

level achieved with stringent, spatially-multimode yet simple and robust filtering. These results outstrip hitherto approaches based on warm-atomic vapours, where quantum correlations could not be demonstrated with many modes and capacity was much smaller^{11,24}. Note that throughout our results no accidental or noise background subtraction is performed, which is in stark contrast to any previous experiments with single-photon sensitive cameras^{11,24,28,29}. In consequence, our setup may be readily applied in a number of quantum imaging experiments such as sub-shot noise imaging⁴⁰.

We achieve the quantum memory lifetime of more than 50 μs which combined with the multimode capacity invites real-time feedback processing of stored excitations⁴². The remaining obstacles on the road to this long-standing goal are mostly linked with the classical feedback bandwidth limited by electronic components such as spatial light modulators and multi-pixel sensors, as the quantum memory elementary operation time of approx. 100 ns is short enough to perform multiple operations within the available storage time. For these reasons we believe that our scheme will promptly enable fast generation of single and multi-photon states^{23,24}.

In particular, here we discuss the application of our scheme as a platform for multi-photon state generation. Figure 1 pictures a protocol utilizing the multi-pixel capability of the single-photon resolving camera to enhance generation of multi-photon states. The essential advantage over recently introduced quantum memory arrays³⁸ is simultaneous excitation and access to many modes. The protocol is being managed by a classical memory storing the wavevectors of registered photons and the which-mode information. This information is finally used to route the photons retrieved in the readout process from the quantum memory. A photonic switch is used to direct photons to a quantum circuit or to conditionally generate arbitrary states through multi-photon interference. Furthermore, since a small number of photons is generated per each frame, one can adapt in real-time the number of trials to create exactly the desired number of excitations in the quantum memory. By keeping the mean photon number per shot small we virtually eliminate the malicious pairs in a single mode. This gives us an advantage over a simpler scheme in which a single excitation shot is used. In that scheme the mean number of photons may be controlled but the multi-mode thermal statistics severely limits the fidelity of generation of n -photon state. Extensions of our new proposal are numerous, including usage of spin-wave echos to conditionally manipulate the atomic excitations⁴³.

RESULTS

Wavevector multiplexing. For the quantum memory we use an engineered atomic ensemble of cold rubidium-87 atoms at $T = 22 \pm 2 \mu\text{K}$ generated within a magneto-optical trap (MOT) and cooled using polarization-gradient cooling (PGC) scheme, as depicted in Fig. 2. With the 1 cm-long cigar-shape

ensemble containing $N = 10^8$ atoms we achieve optical depth $\text{OD} = 40$, which limits the memory readout efficiency^{16,44}. Quantum memory operates once atoms are released from MOT with the magnetic field gradients switched off. We prepare 70% of atoms in the $F = 1, m_F = 1$ state and the rest of atoms in the $F = 1, m_F = 0$ state through optical pumping. Atom-photon interface is achieved with two lasers: write, which is red-detuned from $5^2S_{1/2}, F = 1 \rightarrow 5^2P_{3/2}, F = 2$ transition and read laser tuned to $5^2S_{1/2}, F = 2 \rightarrow 5^2P_{1/2}, F = 2$ transition.

To generate the multimode, multi-photon state we illuminate the ensemble with a write pulse containing 10^7 photons with wavevector \mathbf{k}_w tilted at an angle of 2° to the ensemble axis in the xz plane. We take the axis defined by counter-propagating read and write beams as the z axis of the frame of reference. Stokes (S) photons scattered in the Raman process are registered on the I-sCMOS camera located in the far-field with respect to the atomic ensemble. A scattered photon with a transverse wavevector \mathbf{k}_S is accompanied by a collective atomic excitation (spin-wave) with a spatial phase dependence: $N^{-1/2} \sum_{j=1}^N \exp(i\mathbf{K} \times \mathbf{r}_j) |g_1 \dots h_j \dots g_N\rangle$, where $\mathbf{K} = \mathbf{k}_S - \mathbf{k}_w$ is the spin-wave wavevector, \mathbf{r}_j is the position of j -th atom and summation is carried over all N atoms in the ensemble. To learn about the spin-wave we convert it to an anti-Stokes (AS) photon through resonant Raman scattering (readout process) with a read pulse with wavevector \mathbf{k}_r containing 10^8 photons. Wavevector of the AS photon is determined by the stored atomic excitation $\mathbf{k}_{AS} = \mathbf{K} + \mathbf{k}_r$. We estimate the readout efficiency as $35 \pm 2\%$ (taken as the ratio of coincidence rate to S photons rate and accounted for losses). AS photons are registered on a separate region of the same I-sCMOS sensor.

Spatially-insensitive filtering is essential for the memory to take advantage of its inherent multimode capability. Commonly used frequency filtering cavities^{5,10,12} transmit only one spatial mode. To overcome this issue we use two separate optically-pumped hot rubidium vapor cells with buffer gas and paraffin coating. The cells are pumped by strong lasers during the cooling and trapping period of the MOT. Additional interference filters are used to separate stray pump laser light from single photons (see Methods for details).

Finally, photons originating from the atomic quantum memory are imaged onto the I-sCMOS sensor through a nearly diffraction-limited imaging setup. The sensor is located in the Fourier plane of the atomic ensemble. Positions of photons registered on the camera are calibrated as transverse emission angles, directly proportional to transverse wavevector components. The I-sCMOS camera has the quantum efficiency of 20% and the combined average transmission of the imaging and filtering system is 40% (see Methods for details). The net efficiencies in S and AS arms are equal $\eta_S \approx \eta_{AS} \approx 8\%$,

Data analysis. The spatial degree of freedom provides an advantage over single-mode experiments^{7,8,45}. If

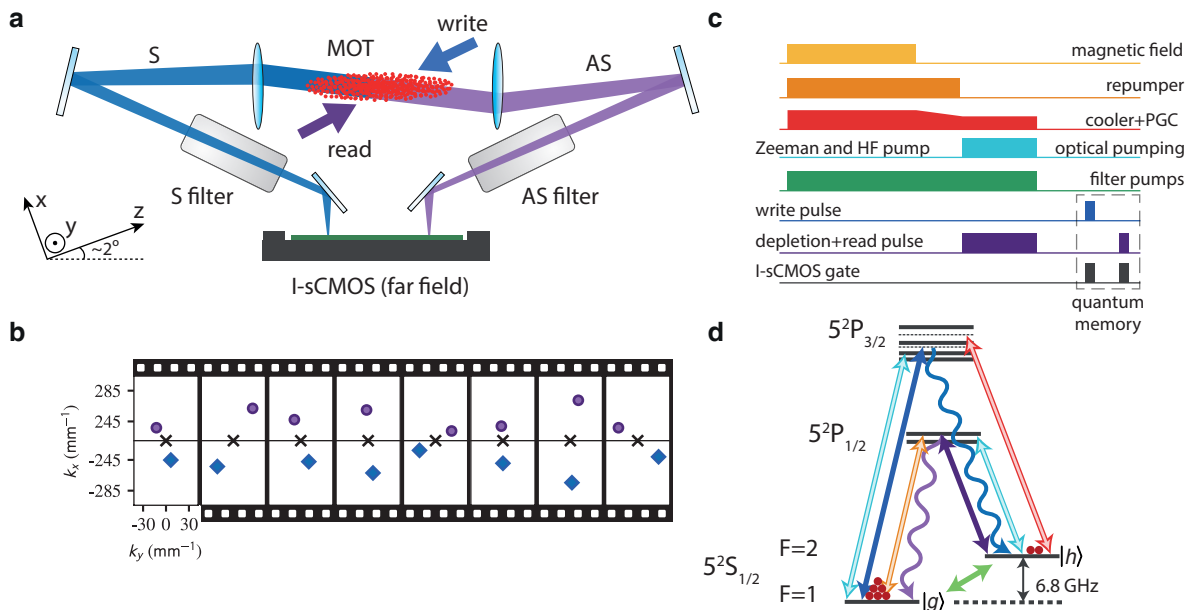


Figure 2. **Experimental realization of the wavevector multiplexed quantum memory.** (a) Schematic of the main part of the experimental setup. The atomic ensemble released from the magneto-optical trap (MOT) is illuminated with orthogonal circularly-polarized write and read laser beams. Angles at which Stokes (S) and anti-Stokes (AS) photons (produced through Raman scattering) are emitted from the atomic ensemble are imaged on the single-photon resolving I-sCMOS sensor, composed of a sCMOS camera and an image intensifier. Optically pumped atomic cells (S and AS filters) filter out the residual laser light and stray fluorescence; (b) Example subsequent frames in the Stokes (bottom) and anti-Stokes (top) regions demonstrating correlated photon pairs in each camera frame. Note that while most frames will contain no photon or a photon only in a single region, almost all ($>90\%$) frames with a coincidence event will contain a correlated photon pair for the detection probability of S photon $p_S = 1.2 \times 10^{-2}$; (c) Pulse sequence used in the experiment (see Methods for details) consists of trapping magnetic field switching, laser cooling and optical pumping (with depletion) preparation stages, as well as short write-in and readout laser pulses (quantum memory stage) producing Stokes and anti-Stokes photons; (d) Atomic level configuration (colors correspond to the pulse sequence in panel c). In the process of write-in and readout the spin-wave (green arrow) is created and annihilated, respectively. The wavy arrows correspond to S (blue) and AS (purple) photons.

one considers each mode as a separate realization of the experiment we are able to collect statistics at a rate of 3×10^5 effective experiments per second. This rate is very similar to what is obtained in single-mode experiments, however the multimode scheme offers much more versatility as increasing the memory storage time to many μs decreases the rate very insignificantly, contrasted with a dramatic drop of the rate in the single-mode experiments. For example with $30 \mu\text{s}$ storage time our experimental rate remains at 300 kHz, while for the single-mode experiment the absolute maximum stands at 33 kHz. Our frame rate is currently limited by the readout speed of the sCMOS camera.

Here, to obtain proper statistics we have collected 10^7 camera frames. For a pair of small conjugate square-shaped region-of-interests (ROI) with side length $\kappa = 160 \text{ mm}^{-1}$ and a net S photon detection probability of 4×10^{-2} we register very few accidental coincidences, i.e. 90% of coincidences come from conjugate modes. This figure of merit changes with a mean photon number and thus the number of observed modes, as due to limited detection efficiencies we will sometimes register a pair of photons from different two different pairwise-coupled

modes. For two conjugate ROIs with a side lengths $\kappa = 340 \text{ mm}^{-1}$ (i.e. 43 mrad) corresponding to a nearly full field of view composed of hundreds of modes we have registered a total number of 1.6×10^5 coincidences of which 4.4×10^4 came from conjugate mode pairs.

Collection of photon counts with a multi-pixel detector requires new experimental and data analysis tools⁴⁶. To verify the anti-correlation between momenta of S and AS photons both in x and y coordinates, we count the coincidences for each pair of camera pixels corresponding to wavevector coordinates $(k_{x,S}, k_{y,S})$ and $(k_{x,AS}, k_{y,AS})$. Figure 3a portrays the number of coincidences for a large field of view as a function of $(k_{y,S}, k_{y,AS})$ momenta summed over the x coordinates. Notably, thanks to a very high signal-to-noise ratio we do not subtract the accidental and noise background in contrast to hitherto schemes^{11,24,28,29}. We observe a clear anti-correlated behavior which we model by the quantum amplitude of the generated Stokes-anti-Stokes photon pair in y dimension, given by:

$$\Psi_y(k_{y,S}, k_{y,AS}) = \mathcal{N} \exp\left(-\frac{(k_{y,S} - k_{y,AS})^2}{2\sigma_y^2}\right), \quad (1)$$

where σ_y is a correlation length in the y dimension and \mathcal{N} is a normalization constant. In turn, the number of coincidences is proportional to $|\Psi_y(k_{y,S}, k_{y,AS})|^2$. An identical expression describes photons behavior in x dimension – see inset in Fig. 3a. For the Gaussian-shaped atomic ensemble the size of the emission mode should be related to ensemble transverse dimension $w = 0.6 \pm 0.1$ mm (taken as $1/e^2$ diameter of the atomic column density), corresponding to wavevector spread of $2/w = 3.3 \pm 0.5$ mm^{-1} in the far-field for light at the wavelength of S photons. To precisely determine the mode widths $\sigma_{x,y}$, in Fig. 3b we plot the coincidences in terms of sum of wavevector variables. Gaussian fit yields values of $\sigma_x = 4.45 \pm 0.02$ mm^{-1} and $\sigma_y = 4.76 \pm 0.02$ mm^{-1} for x and y dimension, respectively. Consequently, we can consider the generated entangled state^{9,11} to be nearly symmetrical in terms of x and y spatial dimensions. This wavevector spread is very close to the limit $2/w$ given by the diffraction at the atomic ensemble and confirms the quality of the imaging system for conjugate modes.

Capacity estimation. From the fundamental point of view multimode states of light can be considered either as continuous-variable systems⁴⁷ or highly-dimensional entangled states⁴⁸ offering large dimensionality of available Hilbert space and in turn providing high informational capacity. Estimation of the informational capacity of continuous-variable entangled states of light has attracted some attention of its own due to broad applications of such states^{11,29}. Various measures of this capacity have been discussed e.g. on the information-theoretical basis⁴⁹. Here we estimate the number of independent mode pairs observed in S and AS arms using the Schmidt mode decomposition^{50,51}. For a single-dimensional photon pair amplitude given by equation (1) and cropped to a finite region we find a decomposition into the Schmidt modes as:

$$\Psi_y(k_{y,S}, k_{y,AS}) = \sum_{j=0}^{\infty} \lambda_j u_j(k_{y,AS}) v_j^*(k_{y,S}), \quad (2)$$

where λ_j are singular values corresponding to contributions of each mode while u_j and v_j^* are orthogonal sets of eigenfunctions. Effective number of independent mode pairs is given by $M = 1/\sum_{j=0}^{\infty} \lambda_j^4$ which may be also described in terms of modes given in an orbital-angular-momentum (OAM)^{7,45,48} or another orthogonal basis. We find the effective number of modes $M_{x,y}$ is well approximated by an inverse relation $M_{x,y} = 0.565 \kappa/2\sigma_{x,y}$ (see Methods for justification) and obtain $M_x = 26.7 \pm 0.1$ and $M_y = 24.9 \pm 0.1$. Finally, for the total number of modes M , which is the product of the number of modes in each spatial dimension, we get $M = M_x M_y = 665 \pm 4$.

Nonclassical photon-number correlations. The presented spatial correlations at a single-photon level require further analysis to confirm actual generation of multi-photon quantum states of light. Quantumness of the correlations (and hence the memory) may be assessed

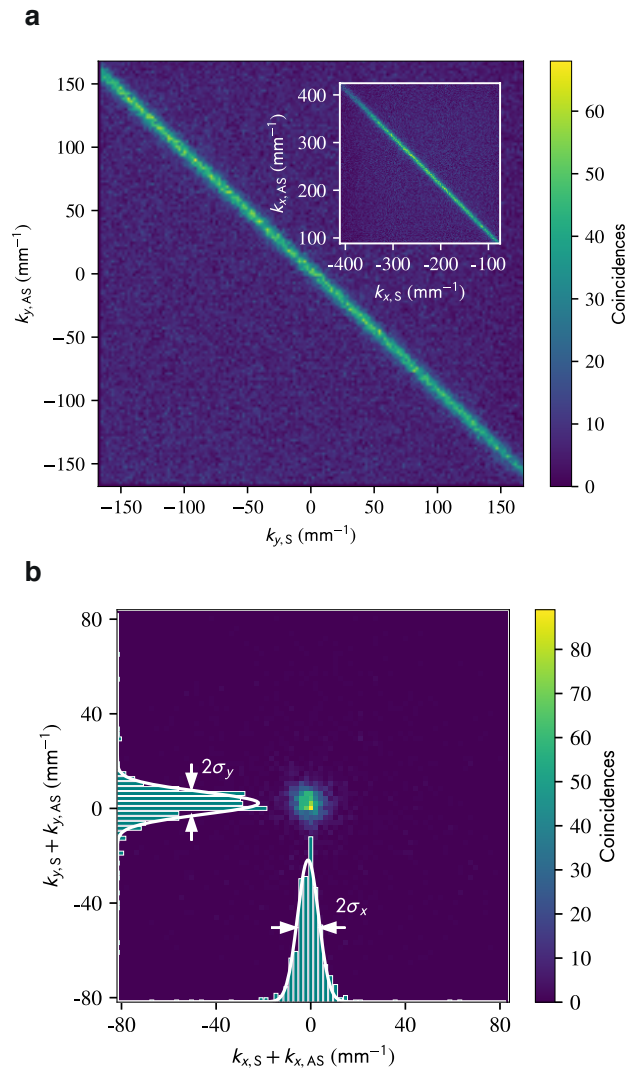


Figure 3. **Spatial properties of the generated biphoton state.** (a) All Stokes–anti-Stokes coincidences marked with their k_y wavevector components (k_x for the inset) for zero memory storage time, demonstrating high degree of momenta anti-correlation. Each plot disregards the perpendicular component. (b) Same coincidences counted in the center-of-mass variables ($k_{x,S} + k_{x,AS}$) and ($k_{y,S} + k_{y,AS}$). The central peak is fitted with a two-dimensional Gaussian to obtain its center and width. One-dimensional distributions correspond to cross-section counts selected for central pixels. Both in (a) and (b) neither accidental nor noise background subtraction is performed.

by looking at the second-order correlation function⁵²:

$$g_{S,AS}^{(2)} = \frac{p_{S,AS}}{p_S p_{AS}}, \quad (3)$$

where p_S and p_{AS} are the probabilities of registering a Stokes and an anti-Stokes photon in their respective regions, while $p_{S,AS}$ is the Stokes–anti-Stokes coincidence probability. Since the single mode statistics of Stokes

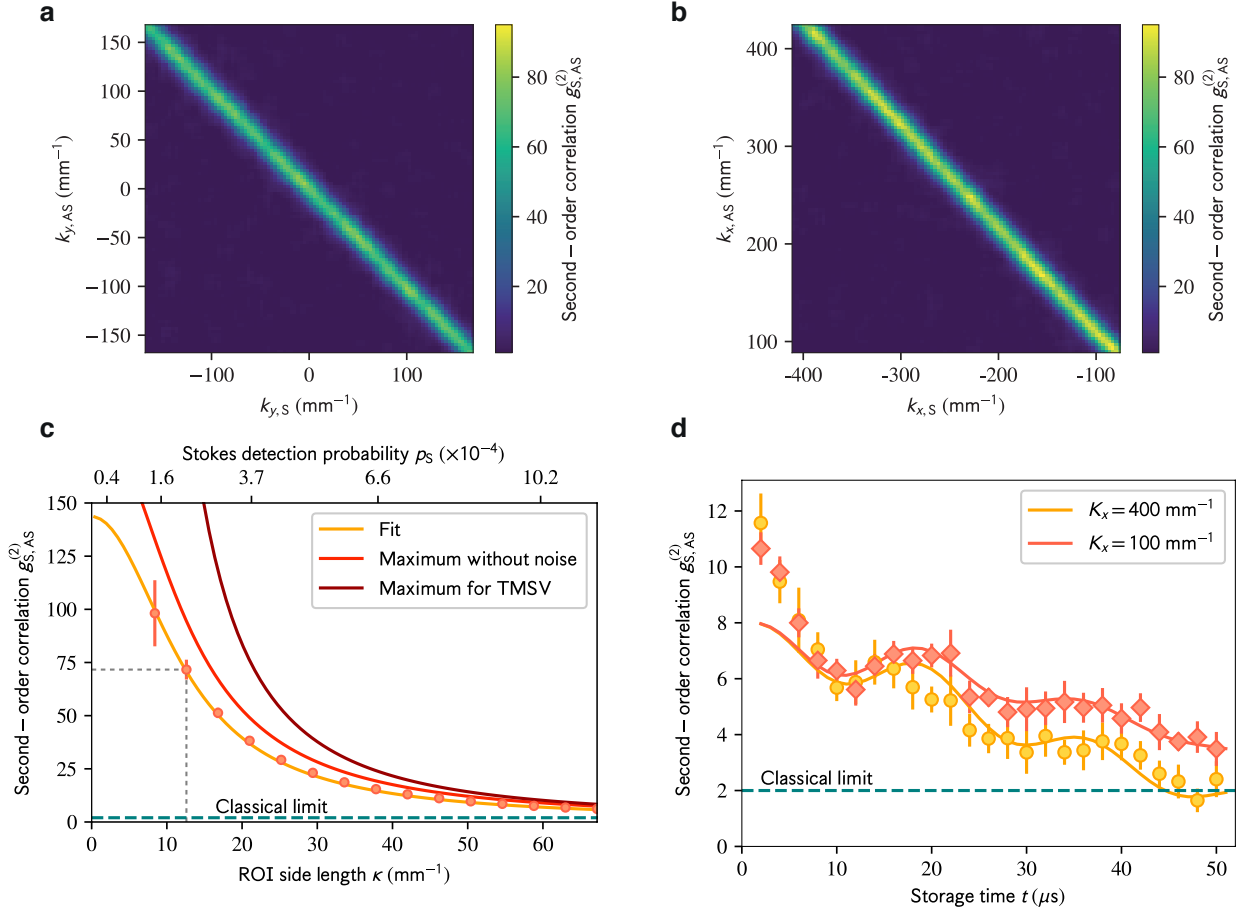


Figure 4. **Nonclassical correlations of photons emitted from the quantum memory.** (a,b) Second-order correlation function $g_{S,AS}^{(2)}$ measured for different positions of ROI in S and AS arms, for zero memory storage time. Nonclassical correlations are observed only between conjugate modes, confirming the highly-multimode character of our quantum memory. Data corresponds to S photon probability $p_S = 2 \times 10^{-4}$ per ROI. (c) $g_{S,AS}^{(2)}$ for Stokes and anti-Stokes photons measured using different sizes of ROI in the analysis. Smaller ROIs correspond to lower p_S and consequently give higher values of $g_{S,AS}^{(2)}$. Our theoretical prediction for the measured mode size closely adheres to experimental results (see Methods for details). Other curves correspond to the maximum value of $g_{S,AS}^{(2)}$ without noise in the AS arm and the maximum theoretical result for two-mode squeezed state (TMSV) with given probability p_S . Grey dashed lines mark the regime of operation used in the measurement shown in (a,b). (d) Second-order correlation as a function of storage time, measured for two different angles of scattering corresponding to stored spin-waves with different K_x . Data was taken with a higher than in (a-c) S photon detection probability of $p_S = 1.9 \times 10^{-3}$ and thus the value of the correlation function is smaller. Nonclassical correlations for spin-waves with smaller wavenumber are confirmed for the storage time t up to 50 μs . Theoretical model (solid lines, see Methods for derivation) exhibits good agreement with experimental data, except for the initial points (see text for details).

and anti-Stokes light are thermal⁵³, the maximum value of local $g_{S,S}^{(2)}$ and $g_{AS,AS}^{(2)}$ autocorrelation functions is 2. Consequently, a value of $g_{S,AS}^{(2)} > 2$ yields violation of the Cauchy-Schwarz inequality and thus proves nonclassical character of the generated state of light.

To perform the measurements we utilize the photon-number resolving capability of the I-sCMOS detector⁴⁶. We verify non-classical photon number correlations in many modes by selecting a set of ROIs in both S and AS arms and calculating $g_{S,AS}^{(2)}$ for all accessible combina-

tions. Results presented in Fig. 4a and b clearly confirm the multimode capacity discussed in previous sections. Next, we select a single pair of square-shaped conjugate ROIs in S and AS arms. Figure 4c presents the measured $g_{S,AS}^{(2)}$ for varying size of ROI with a constant photon flux per pixel. With the decreasing size of ROI the S photon detection probability p_S decreases and we observe $g_{S,AS}^{(2)}$ correlation well above the classical limit of 2 which perfectly matches our theoretical predictions (see Methods for detailed theory of $g_{S,AS}^{(2)}$ measured with a multi-

pixel detector). We compare this result with a maximum value achievable without noise in the AS arm as well as maximum theoretical value for two-mode squeezed state (TMSV) for the given p_S , achievable only if coherent spatial filtering (using e.g. single-mode fibers or cavities) is applied.

Storage capabilities. Cold atomic ensemble prepared in MOT typically offers μs up to ms coherence times, limited mainly by atomic motion, atom losses and stray magnetic fields. We characterize the memory storage time by analyzing the $g_{S,AS}^{(2)}$ correlation function when the read laser is applied after a variable storage time t following the write pulse. Figure 4d presents the average $g_{S,AS}^{(2)}$ calculated for 1,000 pairs of correlated square-shaped ROIs with side length $\kappa = 21 \text{ mm}^{-1}$ and $p_S = 1.9 \times 10^{-3}$ per entire ROI, each comprising approximately 5 modes. Datta sets in Fig. 4d correspond to two different angles at which the photons were scattered, hence spin-waves with different wavevectors — higher scattering angles (and thus spin-waves with larger wavenumbers) correspond to shorter decay times. We observe a quantum-beating oscillation on a double exponential decay of correlations due to the presence of two types of spin-waves arising as a result of imperfect optical pumping (see Methods for details). For all spin-waves we measure lifetimes larger than $60 \mu\text{s}$. In particular for the clock-transition spin-wave (between $F = 1$, $m_F = 1$ and $F = 2$, $m_F = -1$ states) with small $K_x = 100 \text{ mm}^{-1}$ we obtain the lifetime of over $100 \mu\text{s}$. The main source of decoherence is the random atomic motion governed by the Maxwell-Boltzmann velocity distribution⁵⁴. Finally, due to the axial magnetic field of 36 mG, the two types of spin-waves accumulate different phases over the storage time which leads to their constructive or destructive interference at the readout stage. We observe this interference effect as an oscillation with a Larmor period of $T = 2\pi/\omega = 19.5 \mu\text{s}$. The sharp drop in $g_{S,AS}^{(2)}$ in the very beginning (two initial experimental point) is attributed to increase of noise fluorescence as a result of an influx of unpumped thermal atoms into the interaction region. This noise might be eliminated by optical pumping of thermal atoms or by using a two-stage MOT with differential pumping.

DISCUSSION

We have demonstrated a quantum memory-enabled source of spatially-structured nonclassical light based on a principle of wavevector multiplexing. Simultaneous operation on many collective atomic excitations allows us to generate a multimode quantum state of light. The memory preserves nonclassical correlations up to $50 \mu\text{s}$ and exhibits excellent noise properties, in contrast to the previously used warm-atomic vapour schemes^{11,24}. Simultaneous detection using a state-of-the-art single-photon resolving camera is an ideal scheme to implement the enhanced photon generation protocols^{23,24,42}. Our results clearly demonstrate the ability of multimode quantum

memory to emit a single photon with high probability. In particular, we measured S photon detection probability of 0.21 and simultaneously extremely low probability of registering a photon per mode equal 3.8×10^{-4} that drastically minimizes the probability of generating a photon pair in a single mode and proves memory efficacy in enhanced generation of photons. Excellent quality of single photons has been verified through measurements of $g_{S,AS}^{(2)}$ cross-correlation function. Our quantum memory also exhibits an excellent time-bandwidth product of more than 500, which is an important figure of merit in terms of time-bin multiplexing²³. We envisage that hundreds of μs memory lifetime, contrasted with noise-free yet low storage-time solutions⁵⁵, and 100 ns operation time are excellent parameters when it comes to integration with fast electronic or photonic circuits for real-time feedback^{22,56}.

The number of available modes is limited by the imaging system. In a cold atomic ensemble generated within a released MOT we expect the final limit is given by the lifetime of long-wavevector spin-waves as well as phase-matching at the retrieval stage. To keep the lifetime within tens-of-microseconds regime the maximum angle at which the photons are scattered should be smaller than 6 degrees and phase-matching happens to place a similar limitation^{4,57}. Thus we predict that number of readily available modes may reach thousands under the realistic experimental conditions. However, with novel spin-wave manipulation techniques⁵⁸ or by placing the atoms in an optical lattice⁵⁹ at least another order-of-magnitude improvement could be achieved.

While we have focused on the application of our quantum memory as a light source in multiplexed communication and computation protocols^{23,24}, various possible metrological schemes are also worth mentioning. Apart from numerous applications of multi-photon states in quantum-enhanced metrology^{25,26}, spatial photon-number quantum correlations are readily applicable in quantum imaging techniques and the memory capability could help quantum ghost imaging or sub-shot noise imaging along the way to practical applications^{40,41}. Furthermore, the quantum-beat signal between two spin-wave excitations demonstrates the ability of our quantum memory to store a superposition of a few spin-waves in many modes and paves the way towards manipulations within and between the Zeeman sublevels as well as with the spatial degree of freedom.

METHODS

Experimental sequence. Our experimental sequence depicted in Fig. 2c starts with trapping the atoms in MOT for 1.4 ms in an octagonal double-side AR coated glass chamber (Precision Glassblowing) with cooling laser red-detuned from $5^2S_{1/2}$, $F = 2 \rightarrow 5^2P_{3/2}$, $F = 3$ transition by 16 MHz followed by $300 \mu\text{s}$ phase of polarization gradient cooling (PGC, cooling laser detuning increased to 35 MHz by tuning the double-pass acousto-optic modulator) that brings the temperature

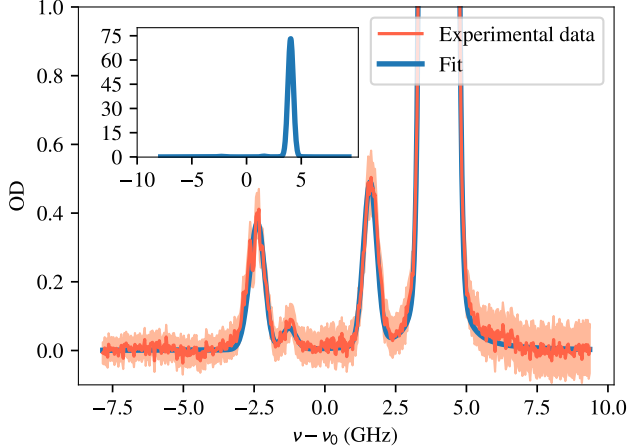


Figure 5. **Characterization of the atomic S filtering system.** Data points correspond to a measurement of absorption of the weak probe beam while fit is the theoretical prediction of OD based on a Voigt-profile absorption model including optical pumping. Inset shows the OD in a larger scale (only the fitted function), demonstrating very high attenuation of write laser light ($\nu - \nu_0 = 4.3$ GHz detuning). Simultaneously, high transmission of S photons ($\nu - \nu_0 = -2.5$ GHz detuning) is achieved. Similar characteristics were also obtained for the AS filter. Detuning is given with respect to the line centroid at ν_0 . Two more central absorption peaks corresponds to a residual amount of ^{85}Rb in the filtering glass cell.

from roughly $100 \mu\text{K}$ to $22 \pm 2 \mu\text{K}$. Fast MOSFET-transistor-based coil switch turns off the coil current in less than $5 \mu\text{s}$ from 125 A to zero. Small stray magnetic fields due to eddy currents take another $200 \mu\text{s}$ to decay but are compensated to nearly zero in the position of the atomic ensemble by a shorted compensation coils, which we verified by taking the free-induction decay measurements⁶⁰. The cooling and trapping period is followed by $40 \mu\text{s}$ stage of optical pumping carried out by three lasers to ensure emptying of the memory state $|h\rangle$ and maximizing of Zeeman population in the $F = 1$, $m_F = 1$ state. Two lasers empty the $F = 2$ manifold: a strong pulse of the read laser (10 mW, depletion stage) as well as another laser (hyperfine pump - HF) tuned to $5^2S_{1/2}$, $F = 2 \rightarrow 5^2P_{1/2}$, $F' = 2$ transition, incident from four directions (with various polarizations) with a total power of 10 mW. Another laser (Zeeman pump) with a power of 7 mW is resonant to $5^2S_{1/2}$, $F = 1 \rightarrow 5^2P_{3/2}$, $F' = 1$ transition and transfers the population from $m_F = -1$ and $m_F = 0$ to $m_F = 1$ state of the $F = 1$ manifold. Dark period of $1 \mu\text{s}$ follows the optical pumping to ensure all light from lasers and from the atomic ensemble is extinguished. Next, a 100 ns write pulse is applied (left-circular polarization, red-detuned by 20 MHz from $5^2S_{1/2}$, $F = 1 \rightarrow 5^2P_{3/2}$, $F' = 2$ transition). After a variable memory storage time a

200 ns read pulse (right-circular polarization, resonant with $5^2S_{1/2}$, $F = 2 \rightarrow 5^2P_{1/2}$, $F = 2$ transition) is applied. All lasers are locked to either cooler or repumper laser through a beat-note offset lock⁶¹.

Imaging. The angles at which the photons are emitted from the atomic ensemble are imaged on the photocathode of the image intensifier with two separate (for S and AS) complex telescopes composed of 6 lenses, each having an effective focal length of $f_{\text{eff}} = 50$ mm. Total length of the single system is 2 m as optically pumped atomic filters need to fit along the photons path. Lens apertures limit our field of view to $2\kappa = 420 \text{ mm}^{-1}$ (for a square ROI) or total solid angle of $\Omega = 2.76$ msr, which later determines maximum number of modes available. The imaging system was calibrated with custom Ronchi rulings. The I-sCMOS device, composed of image intensifier (Hamamatsu V7090D) and a sCMOS sensor (Andor Zyla 5.5 Megapixel), is gated (Photek GM300-3 gating module) only during write-in and readout of atomic excitations. The whole sequence is operated at 500 Hz which is limited by the frame rate of the sCMOS camera. The combined image intensifier gate duration is 400 ns for both write-in and readout stages. The probability of registering a dark count for the combined S and AS fields of view is approx. 5×10^{-3} — much less than typical photon detection probability of 0.2–0.3.

Filtering. Two separate rubidium vapor cells are used to filter out stray write and read laser light from S and AS photons. The 10-cm-long cells are paraffin-coated and contain 99.4% isotopically pure ^{87}Rb as well as buffer gases (Precision Glassblowing, 1 torr Kr for both S and AS filters) that keep the pumped atoms in the interaction region. The cells are pumped with 50 mW of resonant laser light (with $5^2S_{1/2}$, $F = 2 \rightarrow 5^2P_{1/2}$ and $5^2S_{1/2}$, $F = 1 \rightarrow 5^2P_{3/2}$ for S and AS filters, respectively) in a double-pass configuration with collimated 1-cm-wide beams. The optical pumping is active at all times except when the image intensifier gate is open. Importantly, write and read lasers are filtered with Fabry-Pérot cavities before illuminating the ensemble to eliminate amplified spontaneous emission from laser diodes that would not be filtered with the hot atomic cell. Figure 5 presents a characterization of the S filter (we measured the comparable characteristics also for the AS filter). Both filters are characterized by $\text{OD} > 70$ for the laser light and approx. 65% transmission for single photons generated inside the atomic quantum memory.

Coincident counts. Let us consider a collection of M squeezed modes pairs. Assuming the probability p of generating S photon in a single mode and efficiencies in the S and AS arms equal η_S and $\eta_{AS}\chi_R$, respectively, with χ_R being the retrieval efficiency, we obtain the probability of registering a coincidence from any two conjugate modes $pM\eta_S\eta_{AS}\chi_R$. If we now consider a pair of square-shaped ROIs with the side length κ containing M modes for which we again assume the probability p per mode to generate a photon pair, the coincidence rate is reduced, as not all coincidences will fall into the ROI. This effect is

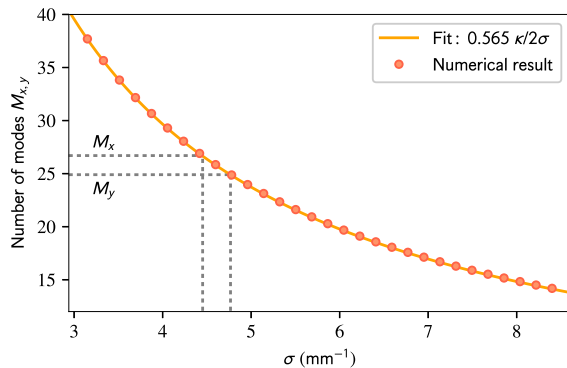


Figure 6. **Result of the eigenmode decomposition for the number of modes.** Dots represent the results from numerical decomposition while the solid line is the simplified prediction of $0.565 \kappa/2\sigma$. Dotted grey lines correspond to values of $\sigma_{x,y}$ we obtain in our experimental setup and corresponding numbers of modes M_x and M_y .

more pronounced for the smaller size of ROI. In particular, if we consider that the S photon is detected inside its respective ROI, we seek the probability that its conjugate AS photon will be detected in conjugate ROI (i.e. with conjugate center). We may calculate this probability by considering photon pairs distributed in momentum space according to equation (1). By considering S photons in the given ROI we calculate the conditional probability $f(\kappa)$ of registering AS photon in the conjugate ROI in the AS arm, which gives us:

$$f(\kappa) = \left(\int_{-\frac{\kappa}{2}}^{\frac{\kappa}{2}} dk_S \int_{-\frac{\kappa}{2}}^{\frac{\kappa}{2}} dk_{AS} \frac{1}{\sqrt{2\pi\kappa\sigma}} e^{-(k_S - k_{AS})^2/2\sigma^2} \right)^2 = \left(\operatorname{erf}\left(\frac{\sqrt{2}\kappa}{2\sigma}\right) + \sqrt{\frac{1}{2\pi}} \frac{2\sigma}{\kappa} \left(e^{-\kappa^2/2\sigma^2} - 1 \right) \right)^2, \quad (4)$$

where squaring is due to the two-dimensional character of the problem. Finally, to estimate the net coincidence probability we additionally consider the total number of accidental coincidences which is very well approximated by a product of probabilities in S and AS arms $p_{SPAS}^{11,21,54,62,63}$. The net S–AS coincidence probability

thus equals:

$$p_{S,AS} = pMf(\kappa)\eta_S\eta_{AS}\chi_R + p_{SPAS}. \quad (5)$$

Second order correlation. We model the evolution of $g_{S,AS}^{(2)}$ correlation function following *Zhao et al.*⁵⁴, but including the effect of interference of different spin-waves as well as the reduced number of coincidence counts due to incoherent spatial filtering. Finally, we end up with the following expression for the second-order correlation function:

$$g_{S,AS}^{(2)} = 1 + \frac{p\eta_S\eta_{AS}\chi_R(t)f(\kappa)}{p\eta_S(p\eta_{AS}\chi_R(t) + \xi)}, \quad (6)$$

where ξ is a contribution of noise in the AS arm. The retrieval efficiency is modeled as an interference of two fields arising due to two atomic coherences by the following time-dependent expression:

$$\chi_R(t) = |\alpha_0 \exp(-t^2/2\tau_1^2) + \alpha_1 \exp(i\omega t) \exp(-t^2/2\tau_2^2)|^2, \quad (7)$$

where α_0 and α_1 are contributions of spin-waves between $F = 1, m_F = 1 \leftrightarrow F = 2, m_F = -1$ and $F = 1, m_F = 0 \leftrightarrow F = 2, m_F = -2$ transitions, respectively. The fit yields $\alpha_0 = 0.58$ and $\alpha_1 = 0.04$, clearly confirming dominant role of the clock-transition spin-wave. The relative phase between the two spin-waves changes as one of them accumulates additional phase due to a Zeeman energy shift $\hbar\omega = 2\pi\hbar \times 51$ kHz in the axial magnetic field of 36 mG. The lifetimes are bounded by wavevector-dependent decoherence rate $\Gamma_D = |\mathbf{K}|v$, with $v = \sqrt{\frac{k_B T}{m_{\text{RB}}}} \approx 1.45$ cm/s.

Eigenmode decomposition. To correctly determine the number of modes we use a similar procedure as proposed by *Law and Eberly*⁵¹. Focusing on one dimension, we generate a normalized biphoton amplitudes according to equation (1), with various widths σ , on a square two-dimensional $k_{y,S} - k_{y,AS}$ grid. We numerically find the eigenmode decomposition of the generated matrix and calculate the number of modes according to equation (2). Figure 6 presents example of results for $\kappa = 420$ mm⁻¹ while the solid line corresponds to a fit of $A\kappa/2\sigma$ relation which we verified numerically for various sets of parameters and obtained $A = 0.565$. Note that for a biphoton amplitude on a rectangular (non-square) grid numerical singular value decomposition (SVD) might be used to give similar results.

-
- [1] Wang, J. *et al.* Terabit free-space data transmission employing orbital angular momentum multiplexing. *Nature Photonics* **6**, 488–496 (2012).
 [2] Richardson, D. J., Fini, J. M. & Nelson, L. E. Space-division multiplexing in optical fibres. *Nature Photonics* **7**, 354–362 (2013).
 [3] Munro, W. J., Harrison, K. A., Stephens, A. M., Devitt, S. J. & Nemoto, K. From quantum fusers to

- high-performance networks. *Nature Photonics* **4**, 792–796 (2010).
 [4] Surmacz, K. *et al.* Efficient spatially resolved multimode quantum memory. *Physical Review A* **78**, 033806 (2008).
 [5] Lan, S.-Y. *et al.* A multiplexed quantum memory. *Optics Express* **17**, 13639–13645 (2009).
 [6] Dai, H.-N. *et al.* Holographic Storage of Biphoton Entanglement. *Physical Review Letters* **108**, 210501 (2012).

- [7] Nicolas, A. *et al.* A quantum memory for orbital angular momentum photonic qubits. *Nature Photonics* **8**, 234–238 (2013).
- [8] Parigi, V. *et al.* Storage and retrieval of vector beams of light in a multiple-degree-of-freedom quantum memory. *Nature Communications* **6**, 7706 (2015).
- [9] Lee, J.-C., Park, K.-K., Zhao, T.-M. & Kim, Y.-H. Einstein-Podolsky-Rosen Entanglement of Narrow-Band Photons from Cold Atoms. *Physical Review Letters* **117**, 250501 (2016).
- [10] Chen, L. *et al.* Controllably releasing long-lived quantum memory for photonic polarization qubit into multiple spatially-separate photonic channels. *Scientific Reports* **6**, 33959 (2016).
- [11] Dąbrowski, M., Parniak, M. & Wasilewski, W. Einstein-Podolsky-Rosen paradox in a hybrid bipartite system. *Optica* **4**, 272–275 (2017).
- [12] Clausen, C. *et al.* Quantum Storage of Photonic Entanglement in a Crystal. *Nature* **469**, 508–511 (2010).
- [13] Collins, M. *et al.* Integrated spatial multiplexing of heralded single-photon sources. *Nature Communications* **4**, 3413–3415 (2013).
- [14] Humphreys, P. C. *et al.* Continuous-variable quantum computing in optical time-frequency modes using quantum memories. *Physical Review Letters* **113**, 130502 (2014).
- [15] Gundogan, M., Ledingham, P. M., Kutluer, K., Mazzer, M. & De Riedmatten, H. Solid State Spin-Wave Quantum Memory for Time-Bin Qubits. *Physical Review Letters* **114**, 230501 (2015).
- [16] Cho, Y. W. *et al.* Highly efficient optical quantum memory with long coherence time in cold atoms. *Optica* **3**, 100–107 (2016).
- [17] Xiong, C. *et al.* Active temporal multiplexing of indistinguishable heralded single photons. *Nature Communications* **7**, 10853 (2016).
- [18] Duan, L.-M., Lukin, M., Cirac, I. & Zoller, P. Long-distance quantum communication with atomic ensembles and linear optics. *Nature* **414**, 413–418 (2001).
- [19] Simon, C. *et al.* Quantum repeaters with photon pair sources and multimode memories. *Physical Review Letters* **98**, 190503 (2007).
- [20] Kutluer, K., Mazzer, M. & de Riedmatten, H. Solid-State Source of Nonclassical Photon Pairs with Embedded Multimode Quantum Memory. *Physical Review Letters* **118**, 210502 (2017).
- [21] Laplane, C., Jobez, P., Etesse, J., Gisin, N. & Afzelius, M. Multimode and Long-Lived Quantum Correlations Between Photons and Spins in a Crystal. *Physical Review Letters* **118**, 210501 (2017).
- [22] Ma, X. S., Zotter, S., Kofler, J., Jennewein, T. & Zeilinger, A. Experimental generation of single photons via active multiplexing. *Physical Review A* **83**, 043814 (2011).
- [23] Nunn, J. *et al.* Enhancing multiphoton rates with quantum memories. *Physical Review Letters* **110**, 133601 (2013).
- [24] Chrapkiewicz, R., Dąbrowski, M. & Wasilewski, W. High-Capacity Angularly Multiplexed Holographic Memory Operating at the Single-Photon Level. *Physical Review Letters* **118**, 063603 (2017).
- [25] Wolgramm, F., Vitelli, C., Beduini, F. A., Godbout, N. & Mitchell, M. W. Entanglement-enhanced probing of a delicate material system. *Nature Photonics* **7**, 28–32 (2012).
- [26] Matthews, J. C. *et al.* Towards practical quantum metrology with photon counting. *npj Quantum Information* **2**, 16023 (2016).
- [27] Kok, P. *et al.* Linear optical quantum computing with photonic qubits. *Reviews of Modern Physics* **79**, 135–174 (2007).
- [28] Edgar, M. *et al.* Imaging high-dimensional spatial entanglement with a camera. *Nature Communications* **3**, 984 (2012).
- [29] Moreau, P. A., Devaux, F. & Lantz, E. Einstein-Podolsky-Rosen Paradox in Twin Images. *Physical Review Letters* **113**, 160401 (2014).
- [30] Krenn, M. *et al.* Generation and confirmation of a (100 x 100)-dimensional entangled quantum system. *Proceedings of the National Academy of Sciences* **111**, 6243–6247 (2014).
- [31] Roslund, J., de Araújo, R. M., Jiang, S., Fabre, C. & Treps, N. Wavelength-multiplexed quantum networks with ultrafast frequency combs. *Nature Photonics* **8**, 109–112 (2013).
- [32] Kaneda, F. *et al.* Time-multiplexed heralded single-photon source. *Optica* **2**, 1010–1013 (2015).
- [33] Xie, Z. *et al.* Harnessing high-dimensional hyperentanglement through a biphoton frequency comb. *Nature Photonics* **9**, 536–542 (2015).
- [34] Reimer, C. *et al.* Generation of multiphoton entangled quantum states by means of integrated frequency combs. *Science* **351**, 1176–1180 (2016).
- [35] Cai, Y. *et al.* Multimode entanglement in reconfigurable graph states using optical frequency combs. *Nature Communications* **8**, 15645 (2017).
- [36] Kaneda, F., Chapman, J., Xu, F. & Kwiat, P. G. Quantum-memory-assisted multi-photon generation for efficient quantum information processing. *arXiv:1704.00879* (2017).
- [37] Tang, J.-S. *et al.* Storage of multiple single-photon pulses emitted from a quantum dot in a solid-state quantum memory. *Nature Communications* **6**, 8652 (2015).
- [38] Pu, Y.-F. *et al.* Experimental realization of a multiplexed quantum memory with 225 individually accessible memory cells. *Nature Communications* **8**, 15359 (2017).
- [39] Boyer, V., Marino, A. M., Pooser, R. C. & Lett, P. D. Entangled Images from Four-Wave Mixing. *Science* **321**, 544–547 (2008).
- [40] Brida, G., Genovese, M. & Ruo Berchera, I. Experimental realization of sub-shot-noise quantum imaging. *Nature Photonics* **4**, 227–230 (2010).
- [41] Genovese, M. Real applications of quantum imaging. *Journal of Optics* **18**, 073002 (2016).
- [42] Mazelanik, M., Dąbrowski, M. & Wasilewski, W. Correlation steering in the angularly multimode Raman atomic memory. *Optics Express* **24**, 21995–22003 (2016).
- [43] Hosseini, M. *et al.* Coherent optical pulse sequencer for quantum applications. *Nature* **461**, 241–5 (2009).
- [44] Zhang, S. *et al.* A dark-line two-dimensional magneto-optical trap of 85Rb atoms with high optical depth. *Review of Scientific Instruments* **83**, 073102 (2012).
- [45] Ding, D.-S., Zhou, Z.-Y., Shi, B.-S., Guo, G.-C. & Harris, S. E. Single-photon-level quantum image memory based on cold atomic ensembles. *Nature Communications* **4**, 183601 (2013).
- [46] Chrapkiewicz, R., Wasilewski, W. & Banaszek, K. High-fidelity spatially resolved multiphoton counting for quan-

- tum imaging applications. *Optics Letters* **39**, 5090–5093 (2014).
- [47] Tasca, D. S., Gomes, R. M., Toscano, F., Souto Ribeiro, P. H. & Walborn, S. P. Continuous-variable quantum computation with spatial degrees of freedom of photons. *Physical Review A* **83**, 052325 (2011).
- [48] Fickler, R., Campbell, G., Buchler, B., Lam, P. K. & Zeilinger, A. Quantum entanglement of angular momentum states with quantum numbers up to 10,010. *Proceedings of the National Academy of Sciences* **113**, 13642–13647 (2016).
- [49] Schneeloch, J., Dixon, P. B., Howland, G. A., Broadbent, C. J. & Howell, J. C. Violation of Continuous-Variable Einstein-Podolsky-Rosen Steering with Discrete Measurements. *Physical Review Letters* **110**, 130407 (2013).
- [50] Grobe, R., Rzażewski, K. & Eberly, J. H. Measure of electron-electron correlation in atomic physics. *Journal of Physics B* **27**, L503–L508 (1999).
- [51] Law, C. K. & Eberly, J. H. Analysis and interpretation of high transverse entanglement in optical parametric down conversion. *Physical Review Letters* **92**, 127903–1 (2004).
- [52] Paul, H. Photon antibunching. *Reviews of Modern Physics* **54**, 1061–1102 (1982).
- [53] Lee, K. C. *et al.* Macroscopic non-classical states and terahertz quantum processing in room-temperature diamond. *Nature Photonics* **6**, 41–44 (2011).
- [54] Zhao, B. *et al.* A millisecond quantum memory for scalable quantum networks. *Nature Physics* **5**, 95–99 (2009).
- [55] Kaczmarek, K. T. *et al.* A room-temperature noise-free quantum memory for broadband light. *arXiv:1704.00013* (2017).
- [56] Hall, M. A., Altepeter, J. B. & Kumar, P. Ultrafast Switching of Photonic Entanglement. *Physical Review Letters* **106**, 053901 (2011).
- [57] Leszczyński, A., Parniak, M. & Wasilewski, W. Phase matching alters spatial multiphoton processes in dense atomic ensembles. *Optics Express* **25**, 284–295 (2017).
- [58] Hétet, G. & Guéry-Odelin, D. Spin wave diffraction control and read-out with a quantum memory for light. *New Journal of Physics* **17**, 073003 (2015).
- [59] Radnaev, A. G. *et al.* A quantum memory with telecom-wavelength conversion. *Nature Physics* **6**, 894–899 (2010).
- [60] Behbood, N. *et al.* Real-time vector field tracking with a cold-atom magnetometer. *Applied Physics Letters* **102**, 173504 (2013).
- [61] Lipka, M., Parniak, M. & Wasilewski, W. Optical Frequency Locked Loop for long-term stabilization of broadband DFB lasers frequency difference. *arXiv:1612.00859* (2016).
- [62] Chen, S. *et al.* Deterministic and storable single-photon source based on a quantum memory. *Phys. Rev. Lett.* **97**, 173004 (2006).
- [63] Albrecht, B., Farrera, P., Heinze, G., Cristiani, M. & de Riedmatten, H. Controlled rephasing of single collective spin excitations in a cold atomic quantum memory. *Phys. Rev. Lett.* **115**, 160501 (2015).

ACKNOWLEDGEMENTS

We acknowledge insightful discussions about the magneto-optical trap with S. Du, G. Campbell, M. Zawada and W. Gawlik, assistance of R. Chrapkiewicz with optical system design, careful proofreading of the manuscript by K. T. Kaczmarek, M. Jachura, R. Chrapkiewicz and M. Semczuk, and generous support of K. Banaszek. The project has been funded by National Science Centre (Poland) grants No. 2015/19/N/ST2/01671, 2016/21/B/ST2/02559 and Polish MNiSW “Diamentowy Grant” Project No. DI2013 011943.

AUTHOR CONTRIBUTIONS

M.P., M.D., M.M. and A.L. performed the experiment and analyzed the data. M.P., M.D. and M.M. wrote the manuscript assisted by other authors. W.W. managed the project. All authors contributed to building of the experimental setup.

CORRESPONDENCE

Correspondence should be addressed to [†]M. Parniak at michal.parniak@fuw.edu.pl or to ^{*}M. Dąbrowski at mdabrowski@fuw.edu.pl.